



HAL
open science

Protein glycation in vivo: Functional and structural effects on yeast enolase

Ricardo A Gomes, Luís M A Oliveira, Mariana C C Silva, Carla Ascenso, Alexandre Quintas, Gonçalo Costa, Ana V Coelho, Marta Sousa Silva, António E N Ferreira, Ana Ponces Freire, et al.

► To cite this version:

Ricardo A Gomes, Luís M A Oliveira, Mariana C C Silva, Carla Ascenso, Alexandre Quintas, et al.. Protein glycation in vivo: Functional and structural effects on yeast enolase. *Biochemical Journal*, 2008, 416 (3), pp.317-326. 10.1042/BJ20080632 . hal-00479002

HAL Id: hal-00479002

<https://hal.science/hal-00479002>

Submitted on 30 Apr 2010

HAL is a multi-disciplinary open access archive for the deposit and dissemination of scientific research documents, whether they are published or not. The documents may come from teaching and research institutions in France or abroad, or from public or private research centers.

L'archive ouverte pluridisciplinaire **HAL**, est destinée au dépôt et à la diffusion de documents scientifiques de niveau recherche, publiés ou non, émanant des établissements d'enseignement et de recherche français ou étrangers, des laboratoires publics ou privés.

Title

Protein glycation *in vivo*: Functional and structural effects on yeast enolase

Running title

Yeast enolase glycation *in vivo*

Ricardo A. Gomes*, Luís M. A. Oliveira^{*,†}, Mariana Silva*, Carla Ascenso[†], Alexandre Quintas[†], Gonçalo Costa[‡], Ana V. Coelho^{‡,§}, Marta Sousa Silva*, António E. N. Ferreira*, Ana Ponces Freire*, Carlos Cordeiro*

* Centro de Química e Bioquímica, Departamento de Química e Bioquímica, Faculdade de Ciências da Universidade de Lisboa, Edifício, Lisboa, Portugal.

† Laboratório de Patologias Neurodegenerativas, Instituto Superior de Ciências da Saúde Egas Moniz, Monte da Caparica, Portugal

‡ Laboratório de Espectrometria de Massa do Instituto de Tecnologia Química e Biológica, Universidade Nova de Lisboa, Oeiras, Portugal

§ Departamento de Química da Universidade de Évora, Portugal

Corresponding author and address:

Carlos Cordeiro

Centro de Química e Bioquímica, Departamento de Química e Bioquímica, Faculdade de Ciências da Universidade de Lisboa, Edifício C8, Lisboa, Portugal.

Fax: 351-217500088

Tel: 351-217500929

caac@fc.ul.pt, url: <http://cqb.fc.ul.pt/enzimol/>

Abbreviations: AGE, advanced glycation end-products; MAGE, methylglyoxal advanced glycation end-products; CD, circular dichroism; MALDI-TOF, matrix assisted laser desorption / ionization - time of flight; HPLC, High performance liquid chromatography; MALDI-FTICR-MS, matrix assisted laser desorption ionization - Fourier transform ion cyclotron resonance mass spectrometry; ESI-FTICR-MS, electrospray ionization - Fourier transform ion cyclotron resonance mass spectrometry; CEL, N^ε-(carboxyethyl)lysine; THP, Tetrahydropyrimidine; MG-H, hydroimidazolone; Argp, Argpyrimidine; TFA, trifluoroacetic acid.

Keywords: MAGE, methylglyoxal, enolase, protein glycation, mass spectrometry, protein structure

SYNOPSIS

Protein glycation is involved in structure and stability changes that impair protein functionality, being associated with several human diseases, like diabetes and amyloidotic neuropathies (Alzheimer, Parkinson and Andrade's syndrome). To understand the relationship of protein glycation with protein dysfunction, unfolding and β -fibril formation, numerous studies have been made *in vitro*. All these previous experiments were conducted in non-physiologic or pseudo physiological conditions that bear little to no resemblance to what may happen in a living cell. *In vivo*, glycation occurs in a crowded and organized environment, where proteins are exposed to a steady state of glycation agents, namely methylglyoxal, while *in vitro*, a bolus of a suitable glycation agent is added to diluted protein samples. Yeast was shown to be an ideal model to investigate glycation *in vivo* since it shows different glycation phenotypes and presents specific protein glycation targets. A comparison between *in vivo* glycated enolase and purified enolase glycated *in vitro* revealed marked differences. All effects regarding structure and stability changes were enhanced when the protein was glycated *in vitro*. The same applies to enzyme activity loss, dimer dissociation and unfolding. However, the major difference lies in the nature and location of specific advanced glycation end-products. *In vivo*, glycation appears to be a specific process, where the same residues are consistently modified in the same way, while *in vitro* several residues are modified with different advanced glycation end-products.

INTRODUCTION

Protein glycation is a non-enzymatic post-translational modification where arginine and lysine side chain amino groups are irreversibly modified by carbonyl compounds, forming advanced glycation end-products (AGE) [1, 2]. Increased protein glycation is associated with several human pathologies like diabetes mellitus and related clinical complications (retinopathy, nephropathy and diabetic vascular diseases) [3], uraemia [4], atherosclerosis [5], age related disorders [3] and neurodegenerative diseases of amyloid type [6-9]. Glycated proteins are present in β -amyloid and τ deposits of Alzheimer's disease [8, 9], in Lewy inclusion bodies of α -synuclein in Parkinson's disease [10], in transthyretin amyloid deposits in familial amyloidotic polyneuropathy [11] and in amyloidotic lateral sclerosis [7]. In all these amyloid pathologies, β -sheet fibril structure and the presence of AGE are common features, suggesting a possible role for glycation in amyloid formation and pathogenesis. In diabetes mellitus and related clinical complications D-glucose was considered to be the main glycation agent leading to irreversible changes in extracellular proteins [3]. However, several lines of evidence suggests that the increased glycation levels observed in several pathological conditions are not directly related to a higher D-glucose concentration but to the increased concentrations of highly reactive low-molecular weight carbonyls compounds, leading to what is described as carbonyl stress [4, 12]. In fact, in several diseases where glycation products accumulate, glycaemia is normal [11]. Moreover, glycation is often found in intracellular proteins, as in Alzheimer's [9] and Parkinson's diseases [10], where D-glucose concentration is negligible. The dicarbonyl compound methylglyoxal is the most significant glycation agent *in vivo*, considering its high reactivity and continuous formation, mainly by the irreversible β -elimination of the phosphate group of dihydroxyacetone phosphate and D-glyceraldehyde-3-phosphate [13-15]. Albeit non-enzymatic, this is a physiological process

that happens alongside glycolysis, hence methylglyoxal formation and protein glycation occur in all living cells. By reacting with the guanine group of arginine, methylglyoxal forms argpyrimidine, hydroimidazolones (MG-H1) and tetrahydropyrimidine (THP) [1, 2]. From its reactions with the ϵ -amino group of lysine, it forms N ^{ϵ} -(carboxyethyl)lysine (CEL) and a methylglyoxal-lysine dimer (MOLD) [1, 2]. These specific markers of protein glycation by methylglyoxal are globally known as methylglyoxal derived advanced glycation end-products, or MAGE. These MAGE has been identified *in vivo* associated with diabetes [16] and in neurodegenerative disorders of amyloid type such as FAP and ALS [7, 11]. Recent evidences suggest that methylglyoxal and not other glycation agents specifically alter the function of several proteins. One example is the specific modification of R188 of Hsp27 with the formation of argpyrimidine, which is essential to the anti-apoptotic activity of this protein [17]. Moreover, glycation by methylglyoxal of small heat-shock proteins appears to be essential for its activation suggesting a mechanism that allows cells to detect and react to carbonyl and unfolding stress [17-20].

Intensive research has been conducted in the last decades whereby the effects of glycation on protein structure and function were investigated in conditions that bear no resemblance at all to what happens *in vivo* [21-24]. Use of concentrations of glycation agents up to the molar range is not uncommon. These studies are in sharp contrast to what happens inside living cells, where methylglyoxal concentration is in the nano to micromolar range, while proteins are in high concentration in a crowded and organized milieu [25]. Consequently, to investigate the effects of glycation on protein structure and function *in vivo*, cellular models must be sought where glycation conditions may be controlled. Yeast offers an ideal cell model to investigate glycation *in vivo*, now that glycation phenotypes and protein glycation targets were uncovered [18, 26, 27]. Among these, enolase2p (2-phospho-D-

glycerate hydrolase, EC 4.2.1.11), the main glycation target, shows a glycation-dependent enzyme activity loss [26].

In this work, a detailed investigation of the effects of methylglyoxal-mediated glycation *in vivo* on the structure, thermal stability and enzyme activity of yeast enolase was performed. MAGE location and identification was made by a bottom-up approach, using MALDI-TOF-MS and high mass accuracy FTICR-MS. Enolase_{2p} was purified from *Saccharomyces cerevisiae* cells in glycation conditions (glycated *in vivo*) and in non-glycation conditions. The native enzyme was modified by methylglyoxal *in vitro*, in conditions often found in the literature. Striking differences between the effects of glycation *in vivo* and *in vitro* were observed. Among these, it is noteworthy the heterogeneity of glycation *in vitro*, whereby different MAGE are often formed at the same lysine or arginine residue, contrasting to the observation that *in vivo* a given MAGE is consistently found at the same amino acid residue.

EXPERIMENTAL

Chemicals and materials

Peptone, yeast extract and agar were from Difco while D-glucose (microbiology grade), KCl and MgSO₄ were obtained from Merck. Ammonium sulphate, NaH₂PO₄, Na₂HPO₄, NaCl, NaF, dithiothreitol, iodoacetamide and TFA were from Sigma. Tris, 20% (w/v) SDS and glycine were from BioRad. EDTA was from BDH chemicals LTD while phosphoenolpyruvate, methylglyoxal 1,1-dimethyl acetal and 2,5 dihydroxybenzoic acid (DHB) were from Fluka. Modified trypsin was from Promega. GELoader tips were from Eppendorf. POROS 10 R2 reversed-phase chromatography medium was from PerSeptive Biosystems. α -Cyano-4-hydroxycinnamic acid (α -CHCA), 3,5 dimethoxy-4-hydroxycinnamic acid (sinapinic acid), PepMix1 (mass spectrometry peptide standards) and ProMix3 (mass spectrometry protein standards) were obtained from LaserBiolabs. Amicon filters were purchased from Millipore. BSA protein digest was from Bruker Daltonics.

Acetonitrile and methanol were HPLC-gradient grade were from Riedel de H en; ultrapure water (type I) was produced in a Millipore Milli-Q system.

Methylglyoxal preparation

Methylglyoxal was prepared by acid hydrolysis of methylglyoxal 1,1-dimethylacetal as reported by Kellum [28] and purified by fractional distillation under reduced pressure in nitrogen atmosphere [29]. Once prepared, methylglyoxal solutions were standardised by enzymatic assay with glyoxalase I and II, as described [30]. Purity was verified by HPLC and NMR analysis on a Bruker Advance 400.

Yeast strains and growth conditions

Saccharomyces cerevisiae strains, Euroscarf collection (Frankfurt, Germany), were: BY4741 (genotype BY4741 *MATa*; *his3Δ1*; *leu2Δ0*; *met15Δ0*; *ura3Δ0*) and ΔGLO1 (isogenic to BY4741 with YML004c::KanMX4). Strains were kept in YPGlu agar slopes [0.5% (w/v) yeast extract, 1% (w/v) peptone, 2% (w/v) agar and 2% (w/v) D-glucose] at 4 °C and cultured in liquid YPGlu medium. To induce protein glycation, ΔGLO1 strain was cultured for 9 days to reach the stationary phase of growth [27]. The reference BY4741 strain was collected at the end of the exponential phase of growth (18 hours).

Enolase purification

Native enolase was purified from BY4741 yeast cells at the end of the exponential phase of growth (18 hours) while glycated enolase was purified from ΔGLO1 culture at the stationary phase (9 days), a condition where glycation was previously observed [27]. Purification was achieved by anion exchange chromatography and size exclusion chromatography after ammonium sulphate protein precipitation from crude extracts, based on a previously described method [31]. Cells were disrupted by sonication (5 cycles of 1 min at 100 Watt with 1 min cooling on ice). The extract was centrifuged at 40000 x g at 4 °C for 30 min to eliminate cell debris and adjusted to 50% saturation of ammonium sulphate. Saturation was subsequently adjusted to 67% by adding solid ammonium sulphate. After centrifugation at 40000 x g at 4 °C for 30 min, the supernatant was made 100% saturated and centrifuged again. The pellet, containing enolase, was resuspended in 20 mM Tris-HCl pH 8.2, containing 5 mM MgSO₄ and 1 mM EDTA. Sample was dialyzed overnight against the same buffer at 4 °C to remove ammonium sulphate and loaded to an ion-exchange chromatography

column DEAE-Sephadex A-50 column equilibrated with 20 mM Tris-HCl, pH 8.2, containing 5 mM MgSO₄ and 1 mM EDTA. Proteins were eluted with a linear NaCl gradient (0–0.5 M) at a flow rate of 1 ml.min⁻¹ and the eluate was monitored at 280 nm. Protein-containing fractions were collected and probed by dot blot analysis using an anti-yeast enolase antibody (a kind gift from Dr. Park, Department of Microbiology, Chungnam National University, Korea). Fractions containing enolase were collected, concentrated by ultrafiltration using Amicon filters and applied to a gel filtration column CM-Sephadex C-50 column, equilibrated with 50 mM NaH₂PO₄:Na₂HPO₄ buffer, pH 7.4 containing 150 mM NaCl, 5 mM MgSO₄ and 1 mM EDTA. Proteins were eluted with the same buffer at a flow rate of 1 ml.min⁻¹. Again, fractions-containing enolase, probed by dot blot, were collected and combined. In the purification of glycosylated enolase, the protein fractions were also probed by dot blot with anti-MAGE antibody (a kind gift from Dr. Ram Nagaraj, Case Western University, Cleveland, Ohio, U.S.A.). Enolase purity was evaluated by SDS-PAGE.

***In vitro* glycation of purified enolase by methylglyoxal**

Purified native enolase (5 μM) was incubated with 10 mM methylglyoxal in 100 mM potassium phosphate buffer, pH 7.4 at 30 °C for 5 days in sterile conditions. Enolase concentration was determined spectrophotometrically ($\epsilon_{280}=0.89 \text{ ml.mg}^{-1}.\text{cm}^{-1}$) [32] in a UV-vis spectrophotometer Jasco V-530.

Western blot and HPLC analysis

Proteins (30 μg protein per lane) were separated by SDS-PAGE in a Mini-protean 3 system (Bio-Rad), using a 12% polyacrylamide separation gel and a 6% polyacrylamide

stacking gel. Proteins were transferred to PVDF membranes (Hybond-P, Amersham Pharmacia Biotech), using the Mini Trans-Blot system (Bio-Rad). Transfer was performed with 39 mM glycine, 48 mM Tris, 0.0375% (w/v) SDS, and 20% (v/v) methanol. Prestained standard proteins (Bio-Rad) were also loaded onto the gel. Total proteins were stained with Ponceau S solution [0.5% (w/v) Ponceau S in 1% (v/v) glacial acetic acid] to confirm protein transfer. For the dot blot assay, purified proteins were applied directly to PVDF membranes previously activated with methanol and equilibrated with transfer buffer. The membranes were blocked overnight at 4 °C in 1% (v/v) blocking solution (Roche) in TBS (50 mM Tris-HCl with 150 mM NaCl, pH 7.5). The anti-MAGE antibody was used diluted 1:5000 in 0.5% (v/v) blocking solution in TBS for 3 hours, while the anti-enolase antibody was used diluted 1:10000 in the same conditions. Washes, secondary antibody and detection procedures were performed using the BM Chemiluminescence Western Blotting Kit (Roche) following manufacturer instructions.

Detection of glycation-induced fluorescence was monitored by reversed phase HPLC on a Beckman-Coulter System Gold equipped with a Beckman-Coulter high-pressure binary gradient pump 126, a Beckman-Coulter 168-diode-array detector (1 nm resolution, 200-600 nm) and a fluorescence detector FP-2020 Plus (Jasco). The mobile phase consisted of 0.08% (v/v) TFA in type I water (solvent A) and 0.08% (v/v) TFA in acetonitrile (solvent B), and the elution gradient program was: 10% to 80% solvent B in 30 min; 80% to 10% solvent B in 10 min. Separation was achieved on a reversed phase analytical column (LiChrospher 100 Merck RP-18, 5 μ m) at a flow rate of 1 ml.min⁻¹. Eluting species were monitored by the fluorescence signal at $\lambda_{em}/\lambda_{exc}$ of 320/385 nm, characteristic of argpyrimidine.

Mass spectrometry analysis

MALDI-TOF mass spectra were acquired in a Voyager-DE STR MALDI-TOF (Applied Biosystems). FTICR-MS mass spectra were obtained in a Bruker Apex Ultra with a 7 Tesla magnet (Bruker Daltonics). For intact protein mass measurement, sinapinic acid (20 mg.ml^{-1}) prepared in 70% (v/v) acetonitrile with 0.1% (v/v) TFA was used as matrix and MALDI-TOF spectra were obtained in positive linear mode. To identify the purified proteins and assign the glycated amino acid residues, peptide mass fingerprint was performed. Protein bands were excised and subjected to reduction, alkylation and digestion with sequencing-grade modified trypsin in gel, according to Pandey and co-workers [33]. The peptide mixture was purified, concentrated by R2 pore microcolumns [34] and eluted directly to the MALDI target plate with $0.8 \mu\text{l}$ of recrystallized matrix α -CHCA (10 mg.ml^{-1}) prepared in 70% (v/v) acetonitrile with 0.1% (v/v) TFA. Monoisotopic peptide masses were used to search for homologies and protein identification with Peptide Mass Fingerprint of Mascot (<http://www.matrixscience.com>). The identification of glycated amino acid residues was performed as described [26]. Briefly, a glycated enolase peptide should have a miscleavage associated with the defined mass increment of a specific MAGE. Moreover, an arginine modification should have a miscleavage in an arginine residue and the same holds true for lysine modifications [26]. The analysis of glycated peptides was also performed by FTICR-MS. In this case, besides in-gel digestion, proteins were hydrolyzed in-solution, essentially as described [35]. The resulting peptide mixture was also purified using PerfectPure C-18 tips (Eppendorf) and diluted in 50% (v/v) methanol with 1% (v/v) formic acid for ESI-FTICR-MS analysis. The peptide mixture was analysed by MALDI-FTICR-MS, using DHB matrix [10 mg.ml^{-1} prepared in 70% (w/v) acetonitrile with 0.1% (v/v) TFA] in an Anchorchip MALDI target (Bruker Daltonics).

Structure and stability analysis

Structural analysis was performed by circular dichroism (CD) spectroscopy and gel filtration chromatography. Prior to CD analysis, individual protein species were separated by gel filtration on an analytical column (Amersham-Pharmacia Superdex™ 75 10/300 GL) with 10 mM phosphate buffer pH 7 containing 100 mM NaF as the mobile phase at a flow rate of 0.4 ml.min⁻¹ (LKB Bromma 2150 isocratic pump with a UV detector JASCO 2075). Eluting peaks were monitored at 280 nm and individual protein fractions were collected for further analysis.

Secondary structure analysis was performed by far-UV (185-240 nm) circular dichroism in a Jasco J810 spectropolarimeter at 25 °C (Julabo F25 temperature control unit) with 0.1 cm path length. CD spectra were deconvoluted using the CDSSTR algorithm [36] on Dichroweb (<http://www.cryst.bbk.ac.uk/cdweb/html/home.html>) [37, 38]. Molar ellipticity was calculated on the basis of a mean residue mass of 107.13 Da. All spectra were solvent baseline-corrected.

Conformational stability measurements were performed by thermal-induced protein unfolding. CD denaturation curves were constructed by raising the temperature from 20 to 85 °C and measuring the ellipticity at 222 nm. The *T_m* value (temperature at which 50% of denaturation occurs) of native and glycosylated enolase was calculated as previously described [39].

Enolase activity assay

Enolase activity was determined at 30 °C in a 1.5 ml reaction volume, on a Beckman DU-7400 diode array spectrophotometer, with temperature control and magnetic stirring,

essential to maintain isotropic conditions during the assay. Enolase activity was followed by measuring phosphoenolpyruvate consumption at 240 nm and its concentration was calculated using $\epsilon = 1.42 \text{ mM}^{-1} \cdot \text{cm}^{-1}$ (this work). The reaction mixture, containing 50 mM Tris-HCl (pH 7.4), 100 mM KCl, 1 mM MgSO_4 , 0.01 mM EDTA and a known amount of protein, was pre-incubated for 10 min and the reaction was started by the addition of phosphoenolpyruvate.

Protein structure

Enolase dimer structure was represented by PDB entry 1ebh. Molecular graphics images were produced using the UCSF Chimera package from the Resource for Biocomputing, Visualization, and Informatics at the University of California, San Francisco (supported by NIH P41 RR-01081) [40]. Relative solvent surface accessibility was calculated according to Gerstein [41].

RESULTS

Characterization of enolase glycation by mass spectrometry

Native enolase was purified from the BY4741 reference strain at the end of the exponential phase of growth and glycated *in vitro* by incubation with 10 mM methylglyoxal in potassium phosphate buffer, a most common glycation condition [42-44]. Purified native enolase also served as a control regarding enzyme activity, secondary structure composition and thermal stability. *In vivo* glycated enolase was purified from the Δ GLO1 strain, lacking the glyoxalase I gene and enzyme activity, hence with higher intracellular methylglyoxal concentration than the reference strain. At the stationary phase of growth, glycation was observed [27]. Protein purity and identity were verified by SDS-PAGE and Western blot analysis with anti-yeast enolase antibody, respectively. Protein identity was further confirmed by peptide mass fingerprint after in gel trypsin digestion and MALDI-TOF analysis of the resulting peptide mixture (data not shown).

As previously shown, peptide mass fingerprint data contains hidden information regarding MAGE nature and location [26]. Since only lysine and arginine residues are modified, tryptic digestion of glycated proteins will produce peptides with at least one miscleavage associated to a defined mass increase corresponding to a specific MAGE (Figure 1). Proteins were also trypsin hydrolyzed in solution to increase the sequence coverage and therefore improve MAGE identification. The resulting peptide mixtures were analyzed by MALDI-TOF, ESI-FTICR-MS and MALDI-FTICR-MS. With the combination of these MS techniques, sequence coverage of about 70% was obtained in all cases.

When enolase is glycated *in vitro*, 10 out of 14 arginine residues are modified by methylglyoxal in the form of hydroimidazolones while only one lysine residue, either K336 or

K337, is modified to CEL, as observed by MALDI-TOF and MALDI-FTICR (Table I). These results are consistent with previous studies that point to hydroimidazolones as the most abundant modifications [45, 46]. The analysis of the in-solution digest by ESI-FTICR-MS also revealed that some arginine residues even form different MAGE on different enolase molecules, like Arg14 which may be modified as hydroimidazolone (observed mass of 2178.056 Da, corresponding to enolase peptide 9-27 with m/z of 2124.045 plus 54.011 Da of a hydroimidazolone modification) or as THP (observed mass of 2268.088 corresponding to the same enolase peptide 9-27 plus 144.042 Da of a THP modification) (Table II). The same MAGE replacement was observed for Arg119 and Arg184 (Table II). This molecular heterogeneity can be seen in a linear mode MALDI-TOF mass spectrum of *in vitro* glycated enolase, showing a large mass increase and peak broadening compared to the molecular mass of native enolase (Figure 2). The formation of different MAGE on the same amino acid residues hints that glycation is not specific *in vitro*. When enolase is glycated *in vivo*, only five arginine residues were found to be modified: Arg402 or Arg405, Arg119 and Arg8 as hydroimidazolones and Arg405 and Arg414 as argpyrimidine (Table I). Only one lysine residue was found as CEL. These modifications appear to be specific since no other MAGE were found at these positions. In this case, the protein molecular mass increase is negligible, as observed by linear mode MALDI-TOF, indicating a lesser glycation extent, and no peak broadening or asymmetry, consistent with a homogeneous distribution of enolase molecular species (Figure 2).

To get insights on the susceptibility of arginine residues towards methylglyoxal-derived glycation, its partial solvent exposure was calculated according to Gerstein [41] (Figure 3). For arginine modifications, no obvious relationship exists between the partial solvent exposure of amino groups and the susceptibility towards glycation. It is quite interesting to notice that arginine residues with reduced surface exposure of both side chain

amino groups, like arginine 119, 391, 405 and 414, are glycosylated. Meanwhile, the two arginine residues that show the highest surface exposure (Arg200 and Arg288) were not found glycosylated. By contrast, solvent exposure appears to be a determinant factor for glycosylation of lysine residues since Lys336 and Lys337 show the highest solvent exposure of all lysine residues in enolase (data not shown).

Glycation effects on enolase folding, structure and enzyme activity

The effects of glycation on enolase structure were evaluated by far-UV circular dichroism spectroscopy after size-exclusion chromatography separation of each molecular form of enolase in solution (native, *in vivo* and *in vitro* glycosylated). Gel filtration chromatograms clearly show two major peaks, one eluting at 20-25 min and the other at 35-40 min (Figure 4A). The first peak corresponds to the enzymatically active enolase dimer (90 kDa) with native secondary structure elements (Figure 4B and C). The second peak immunoreacts with anti-yeast enolase antibody, but shows no CD signal and no enzyme activity, indicating the presence of unfolded, inactive enolase (Figure 4B, C and D). Lack of absorption at 222 nm and 208 nm in the CD spectrum indicates a complete loss of regular secondary structural elements, consistent with the absence of enzyme activity. Similar results were obtained for folded and unfolded protein fractions of glycosylated enolase (data not shown). A comparison of the size exclusion chromatograms shows that, when glycation occurs, a higher fraction of unfolded inactive enolase is observed relatively to the dimeric, folded enzyme (Figure 4A). For native enolase, the unfolded to folded area ratio is about 1 while a two-fold increase of this ratio is observed for *in vivo* glycosylated enolase. When enolase is glycosylated *in vitro*, an even higher amount of unfolded enolase is observed, a nine-fold increase relative to the native enzyme.

If glycation promotes protein dissociation and unfolding, then both protein fractions should be glycosylated. To confirm this hypothesis, these fractions were separated by size exclusion chromatography, analysed by reversed-phase HPLC with fluorescence detection at $\lambda_{\text{ex.320}}\lambda_{\text{em.385}}$ (characteristic of argpyrimidine) and by western blotting using an anti-MAGE antibody. Indeed, both protein fractions derived from enolase glycosylated *in vivo* and *in vitro* contain argpyrimidine and other MAGE (Figure 4E). These results clearly show that enolase glycosylation causes protein unfolding and since glycosylation is an irreversible process, unfolded protein may not be refolded back to the active enzyme form. The effect is far more severe when the protein is glycosylated *in vitro*.

Once the different enolase molecular species were separated by size-exclusion chromatography, samples were analysed by far-UV CD spectroscopy. Striking differences were observed, particularly within the region of 195 nm, 208 nm and 222 nm (Figure 5A). In native enolase, the α -helical content was 40%, β -sheet was 20%, 21% of turns and 19% of unordered structure (Table III). These values are in agreement with the values of 37.6% for α -helix, 21% of β -sheet, 26% of turns and 15.4% unordered structures obtained by Fourier transformed infrared spectroscopy [32]. X-Ray crystallography analysis of yeast enolase, estimated an α -helical content of 37.3% and 17.2% of β -sheet [47]. *In vivo* glycosylated enolase shows little to no secondary structure loss. However, a redistribution of secondary structure elements is evident, with an increase of unordered structure from 19% to 25%, a reduction of the α -helical content from 40% to 35%, while β -sheet content remains unchanged (Table III). When enolase is glycosylated *in vitro*, a distinct scenario emerges. There is a much higher loss of α -helix content, from 40% to 17%, and a large increase of β -sheet, from 20% to 32%, compared to *in vivo* glycosylated enolase (Table III). Unordered structure elements also increase, from 19% to 32%.

To evaluate the glycation effects on the structural stability of enolase, thermal denaturation of the native, *in vivo* and *in vitro* glycated enolase was monitored by CD spectroscopy. Glycation shifts the thermal denaturation curve of enolase to higher temperatures, indicating an increased resistance to thermal unfolding (Figure 5B). In fact, the T_m for native enolase is 53.6 °C while *in vivo* glycated enolase shows a T_m of 58.6 °C and the *in vitro* glycated enolase an even higher T_m of 61.4 °C. Enolase thermal denaturation is an irreversible process, as confirmed by protein aggregation and lack of secondary structure analysed by CD when the temperature was returned to 25 °C (data not shown), hence the determination of thermodynamic parameters could not be performed.

Secondary structure changes are associated with protein function modifications. Therefore, glycation-induced conformational changes are likely to have pronounced effects on enolase activity. Indeed, we observed a marked decrease in enolase activity upon glycation (Figure 6). *In vivo* glycated enolase shows a 65% activity loss compared to native enolase. When enolase is glycated *in vitro*, an even more severe activity loss is observed (84%). As glycation causes enolase denaturation with a consequent enzyme inactivation, it could be argued that the loss of enzyme specific activity may be solely explained by the higher amount of unfolded inactive protein in the sample. This implies that, if the activity of glycated folded enolase remains the same, the specific activity would decrease. To investigate this hypothesis, folded and unfolded fractions from *in vivo* and *in vitro* glycated enolase were separated by size exclusion chromatography and enzyme activity was determined for each individual fraction (fraction I being folded active and glycated enolase while fraction II is unfolded glycated enolase). In both cases, no enolase activity was detected in fraction II, consistent with the lack of secondary structure. In fraction I, enolase activity was detected, albeit the specific activity was again much lower than that of the native enzyme (Figure 6).

DISCUSSION

Arginine residues have a probability of about 20% to be located in ligand and substrate binding sites of proteins [48]. Hence, methylglyoxal-derived arginine glycation is expected to have significant effects on protein structure and function, being related to several human pathologies [3, 4, 8, 10, 11]. Therefore, this post-translational modification has been the subject of an intensive research, where *in vitro* glycation of clinically relevant and model proteins were investigated [22, 23, 45]. The major drawback of this approach lies on the dramatic differences between glycation conditions *in vitro* and *in vivo*. *In vitro*, non-physiological concentrations of glycation agents are used, from millimolar to molar concentrations [21-24]. Additionally, protein interactions are not taken into account. Also, protein turnover and the action of molecular chaperones, some of which are activated upon glycation by methylglyoxal [19, 20, 26] is absent. These differences highlight the importance of investigating protein glycation mechanisms and their biochemical effects *in vivo*. Our previous studies validated yeast as a eukaryotic cell model to investigate protein glycation *in vivo* [26, 27]. Enolase, the major glycation target, shows glycation-dependent activity loss [26], providing an important model to study glycation effects *in vivo*.

In agreement with our hypothesis that protein glycation is different *in vivo* and *in vitro*, mass spectrometry analysis indicates that enolase glycation *in vivo* is site-specific whereby only a few amino acid residues are consistently modified with the same MAGE. By contrast, glycation *in vitro* is a heterogeneous process, resulting in the formation of a complex population of enolase molecules with different glycation profiles. *In vitro*, different MAGE may be present at the same arginine residue, in different protein molecules. Glycation specificity not related to the partial solvent exposure of arginine residues (Fig. 3). We previously suggested that the arginine-rich deep crevice in enolase protein structure,

accessible to the solvent and located at the dimer interface, may be a favourable hotspot for the occurrence of glycation [26]. Several glycosylated arginine residues identified after *in vitro* glycation and almost all glycosylated arginines *in vivo* are located in this cleft (Figure 7A and B). Interestingly, glycation was not detected in the two most exposed arginine residues (R200 and R288), outside the cleft (Figure 7C).

In vivo glycosylated enolase shows an increase of unordered structure. α -Helical content decreases and T_m increases with glycation, suggesting that glycosylated enolase may exist in a more compact and rigid conformation. When enolase was glycosylated *in vitro*, besides an enhanced increase of unordered structure and a decrease of α -helix, a marked gain of β -sheet was also observed. The T_m increase is more pronounced, consistent with an even more rigid structure, probably due to higher β -sheet content.

Glycation also leads to enolase unfolding. This is in agreement with our previous model of glycation-induced enolase inactivation in which the glycation of the critical arginine residue 414 disrupted an ionic pair formed with glutamate residue 20, essential for dimer stability [26]. A modification of R414 was observed in this study, both consequence of *in vivo* and *in vitro* glycation. When enolase is glycosylated *in vitro*, unfolding is much more pronounced. This can be due to the higher glycation extent or because the molecular chaperone pathway which is activated by glycation *in vivo* is absent from a test tube [19, 26]. The observed changes in protein structure and stability are related to the glycation-dependent activity loss, 65% inactivation *in vivo* and 85% activity loss *in vitro*.

The results presented reveal important differences between glycation *in vivo* and *in vitro* in the conditions used, which may be related to diverse glycation specificities. This observation highlights the importance of investigating protein glycation *in vivo* in a model system such as yeast, already validated in the research of amyloidotic neurodegenerative diseases [49].

ACKNOWLEDGEMENTS

We thank Dr. H.M. Park for the gift of the anti-yeast-enolase polyclonal antibody and Dr. Ram Nagaraj for the gift of the anti-MAGE antibody. We wish to acknowledge Dr. Ana Varela Coelho for providing data from the Laboratório de espectrometria de massa at the Instituto de Tecnologia Química e Biológica, Universidade Nova de Lisboa, Oeiras, Portugal. Work supported by grants SFRH/BD/13884/2003 (R.A.G.), SFRH/BPD/28345/2006 (M.S.S.) and SFRH/BD/23604/2005 (L.O.) from the Fundação para a Ciência e a Tecnologia, Ministério da Ciência e Tecnologia, Portugal.

REFERENCES

- 1 Westwood, M. E. and Thornalley, P. J. (1997) Glycation and Advanced Glycation Endproducts. In *The Glycation Hypothesis of Atherosclerosis* (Colaco, C., ed.). pp. 57-87
- 2 Grillo, M. A. and Colombatto, S. (2008) Advanced glycation end-products (AGEs): involvement in aging and in neurodegenerative diseases. *Amino Acids*. **35**, 29-36
- 3 Brownlee, M. (1995) Advanced protein glycosylation in diabetes and aging. *Annu. Rev. Med.* **46**, 223-234
- 4 Miyata, T., Ueda, Y., Saito, A. and Kurokawa, K. (2000) 'Carbonyl stress' and dialysis-related amyloidosis. *Nephrol. Dial. Transplant.* **15 Suppl 1**, 25-28
- 5 Kume, S., Takeya, M., Mori, T., Araki, N., Suzuki, H., Horiuchi, S., Kodama, T., Miyauchi, Y. and Takahashi, K. (1995) Immunohistochemical and ultrastructural detection of advanced glycation end products in atherosclerotic lesions of human aorta with a novel specific monoclonal antibody. *Am. J. Pathol.* **147**, 654-667
- 6 Miyata, T., Inagi, R., Iida, Y., Sato, M., Yamada, N., Oda, O., Maeda, K. and Seo, H. (1994) Involvement of beta 2-microglobulin modified with advanced glycation end products in the pathogenesis of hemodialysis-associated amyloidosis. Induction of human monocyte chemotaxis and macrophage secretion of tumor necrosis factor-alpha and interleukin-1. *J. Clin. Invest.* **93**, 521-528
- 7 Shibata, N., Hirano, A., Hedley-Whyte, E. T., Dal Canto, M. C., Nagai, R., Uchida, K., Horiuchi, S., Kawaguchi, M., Yamamoto, T. and Kobayashi, M. (2002) Selective formation of certain advanced glycation end products in spinal cord astrocytes of humans and mice with superoxide dismutase-1 mutation. *Acta Neuropathol. (Berl)*. **104**, 171-178
- 8 Vitek, M. P., Bhattacharya, K., Glendening, J. M., Stopa, E., Vlassara, H., Bucala, R., Manogue, K. and Cerami, A. (1994) Advanced glycation end products contribute to amyloidosis in Alzheimer disease. *Proc. Natl. Acad. Sci. U S A.* **91**, 4766-4770
- 9 Yan, S. D., Chen, X., Schmidt, A. M., Brett, J., Godman, G., Zou, Y. S., Scott, C. W., Caputo, C., Frappier, T. and Smith, M. A. (1994) Glycated tau protein in Alzheimer disease: a mechanism for induction of oxidant stress. *Proc. Natl. Acad. Sci. U S A.* **91**, 7787-7791
- 10 Castellani, R., Smith, M. A., Richey, P. L. and Perry, G. (1996) Glycooxidation and oxidative stress in Parkinson disease and diffuse Lewy body disease. *Brain Res.* **737**, 195-200
- 11 Gomes, R., Sousa Silva, M., Quintas, A., Cordeiro, C., Freire, A., Pereira, P., Martins, A., Monteiro, E., Barroso, E. and Ponces Freire, A. (2005) Argpyrimidine, a methylglyoxal-derived advanced glycation end-product in familial amyloidotic polyneuropathy. *Biochem. J.* **385**, 339-345
- 12 Baynes, J. W. and Thorpe, S. R. (1999) Role of oxidative stress in diabetic complications: a new perspective on an old paradigm. *Diabetes.* **48**, 1-9
- 13 Richard, J. P. (1984) Acid-Base Catalysis of the Elimination and Isomerization-Reactions of Triose Phosphates. *Journal of the American Chemical Society.* **106**, 4926-4936
- 14 Richard, J. P. (1993) Mechanism for the formation of methylglyoxal from triosephosphates. *Biochem. Soc. Trans.* **21**, 549-553
- 15 Thornalley, P. J. (1996) Pharmacology of methylglyoxal: formation, modification of proteins and nucleic acids, and enzymatic detoxification--a role in pathogenesis and antiproliferative chemotherapy. *Gen. Pharmacol.* **27**, 565-573

- 16 Kilhovd, B. K., Giardino, I., Torjesen, P. A., Birkeland, K. I., Berg, T. J., Thornalley, P. J., Brownlee, M. and Hanssen, K. F. (2003) Increased serum levels of the specific AGE-compound methylglyoxal-derived hydroimidazolone in patients with type 2 diabetes. *Metabolism*. **52**, 163-167
- 17 Sakamoto, H., Mashima, T., Yamamoto, K. and Tsuruo, T. (2002) Modulation of heat-shock protein 27 (Hsp27) anti-apoptotic activity by methylglyoxal modification. *J. Biol. Chem.* **277**, 45770-45775
- 18 Gomes, R. A., Miranda, H. V., Sousa Silva, M., Graca, G., Coelho, A. V., do Nascimento Ferreira, A. E., Cordeiro, C. and Freire, A. P. (2008) Protein glycation and methylglyoxal metabolism in yeast: finding peptide needles in protein haystacks. *FEMS Yeast Res.* **8**, 174-181
- 19 Nagaraj, R. H., Oya-Ito, T., Padayatti, P. S., Kumar, R., Mehta, S., West, K., Levison, B., Sun, J., Crabb, J. W. and Padival, A. K. (2003) Enhancement of chaperone function of alpha-crystallin by methylglyoxal modification. *Biochemistry*. **42**, 10746-10755
- 20 Oya-Ito, T., Liu, B. F. and Nagaraj, R. H. (2006) Effect of methylglyoxal modification and phosphorylation on the chaperone and anti-apoptotic properties of heat shock protein 27. *J. Cell Biochem.* **99**, 279-291
- 21 Bakhti, M., Habibi-Rezaei, M., Moosavi-Movahedi, A. A. and Khazaei, M. R. (2007) Consequential Alterations in Haemoglobin Structure upon Glycation with Fructose: Prevention by Acetylsalicylic Acid. *J. Biochem. (Tokyo)*. **141**, 827-833
- 22 Bouma, B., Kroon-Batenburg, L. M., Wu, Y. P., Brunjes, B., Posthuma, G., Kranenburg, O., de Groot, P. G., Voest, E. E. and Gebbink, M. F. (2003) Glycation induces formation of amyloid cross-beta structure in albumin. *J. Biol. Chem.* **278**, 41810-41819
- 23 Luthra, M. and Balasubramanian, D. (1993) Nonenzymatic glycation alters protein structure and stability. A study of two eye lens crystallins. *J. Biol. Chem.* **268**, 18119-18127
- 24 Seidler, N. W. and Kowalewski, C. (2003) Methylglyoxal-induced glycation affects protein topography. *Arch. Biochem. Biophys.* **410**, 149-154
- 25 Srere, P. A. (1987) Complexes of sequential metabolic enzymes. *Ann. Rev. Biochem.* **56**, 89-124
- 26 Gomes, R. A., Miranda, H. V., Silva, M. S., Graca, G., Coelho, A. V., Ferreira, A. E., Cordeiro, C. and Freire, A. P. (2006) Yeast protein glycation *in vivo* by methylglyoxal. Molecular modification of glycolytic enzymes and heat shock proteins. *Febs J.* **273**, 5273-5287
- 27 Gomes, R. A., Sousa Silva, M., Vicente Miranda, H., Ferreira, A. E., Cordeiro, C. A. and Freire, A. P. (2005) Protein glycation in *Saccharomyces cerevisiae*. Argpyrimidine formation and methylglyoxal catabolism. *Febs J.* **272**, 4521-4531
- 28 Kellum, M. W., Oray, B. and Norton, S. J. (1978) A convenient quantitative synthesis of methylglyoxal for glyoxalase I assays. *Anal. Biochem.* **85**, 586-590
- 29 McLellan, A. C., Phillips, S. A. and Thornalley, P. J. (1992) The assay of methylglyoxal in biological systems by derivatization with 1,2-diamino-4,5-dimethoxybenzene. *Anal. Biochem.* **206**, 17-23
- 30 Racker, E. (1951) The mechanism of action of glyoxalase. *J. Biol. Chem.* **190**, 685-696
- 31 Kustrzeba-Wojcicka, I. and Golczak, M. (2000) Enolase from *Candida albicans*-purification and characterization. *Comp. Biochem. Physiol. B Biochem. Mol. Biol.* **126**, 109-120

- 32 Huang, P. and Dong, A. (2003) Thermal, chemical and chemothermal denaturation of yeast enolase. *Spectroscopy*. **17**, 453-467
- 33 Pandey, A., Andersen, J. S. and Mann, M. (2000) Use of mass spectrometry to study signaling pathways. *Sci. STKE*. **2000**, PL1
- 34 Gobom, J., Nordhoff, E., Mirgorodskaya, E., Ekman, R. and Roepstorff, P. (1999) Sample purification and preparation technique based on nano-scale reversed-phase columns for the sensitive analysis of complex peptide mixtures by matrix-assisted laser desorption/ionization mass spectrometry. *J. Mass Spectrom.* **34**, 105-116
- 35 Olsen, J. V. and Mann, M. (2004) Improved peptide identification in proteomics by two consecutive stages of mass spectrometric fragmentation. *Proc. Natl. Acad. Sci. U S A*. **101**, 13417-13422
- 36 Johnson, W. C. (1999) Analyzing protein circular dichroism spectra for accurate secondary structures. *Proteins*. **35**, 307-312
- 37 Lobley, A., Whitmore, L. and Wallace, B. A. (2002) DICHROWEB: an interactive website for the analysis of protein secondary structure from circular dichroism spectra. *Bioinformatics*. **18**, 211-212
- 38 Whitmore, L. and Wallace, B. A. (2004) DICHROWEB, an online server for protein secondary structure analyses from circular dichroism spectroscopic data. *Nucleic Acids Res.* **32**, W668-673
- 39 Pace, C. N., Shirley, B. A. and Thomson, J. A. (1990) Measuring the conformational stability of a protein. In *In protein structure: a practical approach* (Creighton, T. E. E., ed.). pp. 311-330, Oxford University Press, Oxford UK
- 40 Pettersen, E. F., Goddard, T. D., Huang, C. C., Couch, G. S., Greenblatt, D. M., Meng, E. C. and Ferrin, T. E. (2004) UCSF Chimera—a visualization system for exploratory research and analysis. *J. Comput. Chem.* **25**, 1605-1612
- 41 Gerstein, M. (1992) A resolution-sensitive procedure for comparing protein surfaces and its application to the comparison of antigen-combining sites. *Acta Cryst. A*. **48**, 271
- 42 Kang, J. H. (2003) Modification and inactivation of human Cu,Zn-superoxide dismutase by methylglyoxal. *Mol. Cells*. **15**, 194-199
- 43 Shipanova, I. N., Glomb, M. A. and Nagaraj, R. H. (1997) Protein modification by methylglyoxal: chemical nature and synthetic mechanism of a major fluorescent adduct. *Arch. Biochem. Biophys.* **344**, 29-36
- 44 Ahmed, M. U., Brinkmann Frye, E., Degenhardt, T. P., Thorpe, S. R. and Baynes, J. W. (1997) N-epsilon-(carboxyethyl)lysine, a product of the chemical modification of proteins by methylglyoxal, increases with age in human lens proteins. *Biochem. J.* **324** (Pt 2), 565-570
- 45 Ahmed, N., Dobler, D., Dean, M. and Thornalley, P. J. (2005) Peptide mapping identifies hotspot site of modification in human serum albumin by methylglyoxal involved in ligand binding and esterase activity. *J. Biol. Chem.* **280**, 5724-5732
- 46 Ahmed, N., Thornalley, P. J., Dawczynski, J., Franke, S., Strobel, J., Stein, G. and Haik, G. M. (2003) Methylglyoxal-derived hydroimidazolone advanced glycation end-products of human lens proteins. *Invest. Ophthalmol. Vis. Sci.* **44**, 5287-5292
- 47 Stec, B. and Lebioda, L. (1990) Refined structure of yeast apo-enolase at 2.25 Å resolution. *J. Mol. Biol.* **211**, 235-248
- 48 Gallet, X., Charlotiaux, B., Thomas, A. and Brasseur, R. (2000) A fast method to predict protein interaction sites from sequences. *J. Mol. Biol.* **302**, 917-926
- 49 Outeiro, T. F. and Lindquist, S. (2003) Yeast cells provide insight into alpha-synuclein biology and pathobiology. *Science*. **302**, 1772-1775

TABLES AND FIGURE LEGENDS

Table I. Chemical identification and molecular localization of MAGE in enolase by MALDI-TOF and MALDI-FTICR mass spectrometry. Glycated residues are underlined. MG-H, hydroimidazolone; Argp, argpyrimidine; CEL, N^ε-(carboxyethyl)lysine.

Table II. Identification and localization of MAGE in enolase glycated *in vitro* by methylglyoxal using ESI-FTICR-MS. Glycated residues are underlined. Noticeably, the same glycated amino acid residue appears with different chemical modifications. MG-H, hydroimidazolone; THP, tetrahydropyrimidine.

Table III. Distribution of secondary structure elements for native, *in vivo* and *in vitro* glycated enolase, obtained by CD spectra deconvolution with the CDSSTR algorithm (Dichroweb; <http://www.cryst.bbk.ac.uk/cdweb/html/home.html>). The NRMSD parameter is the normalized root mean square deviation.

Figure 1. Chemical detection and molecular location of MAGE in enolase. Glycated peptides show miscleavages associated with specific mass increments characteristics of a given MAGE [26]. Figure shows sections of MALDI-TOF mass spectrum where the appearance of new peptides with MAGE in enolase glycated *in vivo* (A) and *in vitro* (B) are observed, in comparison with the native protein. The complete analysis of the mass spectrometry data is presented on table II and III.

Figure 2. Analysis of intact protein mass by linear MALDI-TOF of native (A), *in vitro* glycated (B) and *in vivo* glycated enolase (C). For all mass spectra, a peak with m/z similar to

theoretical yeast enolase 2 molecular mass (46 782 Da) was obtained. With glycation *in vitro*, a broadening of the peak is observed indicating higher sample heterogeneity.

Figure 3. Surface exposure of arginine side chain in yeast enolase, calculated according to Gerstein [41]. Glycated and non-glycated arginine residues are shown.

Figure 4. Characterization of the different enolase species. A) Size exclusion chromatography of native, glycated *in vivo* and glycated *in vitro* enolase, showing the presence of two major protein fractions (marked as fraction I and II). B) Far-UV CD spectra of fraction I (black) and fraction II (light gray) collected from gel filtration of native enolase. Contrary to fraction I, no CD signal was observed in fraction II, showing a complete loss of secondary structure elements. C) Enolase activity assays of fraction I (black) and II (light gray). Consistent with the lack of secondary structure, no enzyme activity was detected in fraction II. D) Dot-blot analysis of both fractions with anti-yeast enolase antibody, with positive results. E) Glycation analysis by HPLC and dot-blot of fraction I (black) and fraction II (light gray) from enolase glycated *in vivo*. Both fractions show a fluorescent peak around 6 min at wavelengths characteristic of argpyrimidine ($\lambda_{ex.320}/\lambda_{em.385}$) indicating that both fractions are glycated. The positive signal obtained by dot-blot analysis with anti-MAGE antibody also indicates that both fractions are glycated.

Figure 5. Enolase structure and stability. A) Far-UV CD spectra of native, *in vivo* glycated and *in vitro* glycated enolase between 185 and 240 nm. B) Thermal denaturation of native, *in vivo* and *in vitro* glycated enolase. Upon glycation, a shift towards higher melting temperatures is observed.

Figure 6. Glycation effects on enolase activity. Enolase activity was determined by the consumption of phosphoenolpyruvate, as described. Glycation induces a considerable activity loss. Fraction I contains folded active enolase. Data shown are averages from three independent activity assays \pm SD.

Figure 7. Surface landscape of dimeric yeast enolase, showing the glycosylated (red) and non-glycosylated (yellow) arginine residues. For greater clarity, the surface of one of the subunits is shown in light gray. A) Enolase glycosylated *in vitro* showing glycosylated arginine residue in a cleft at the dimer interface. B) *In vivo* glycosylated enolase showing four out of five glycosylated arginine residues in the cleft between the two monomers. C) Enolase structure showing the highest solvent exposed arginine residues R200 and R288 that were not glycosylated. Interestingly, these arginine residues are not located at the dimer interface.

Figure 1

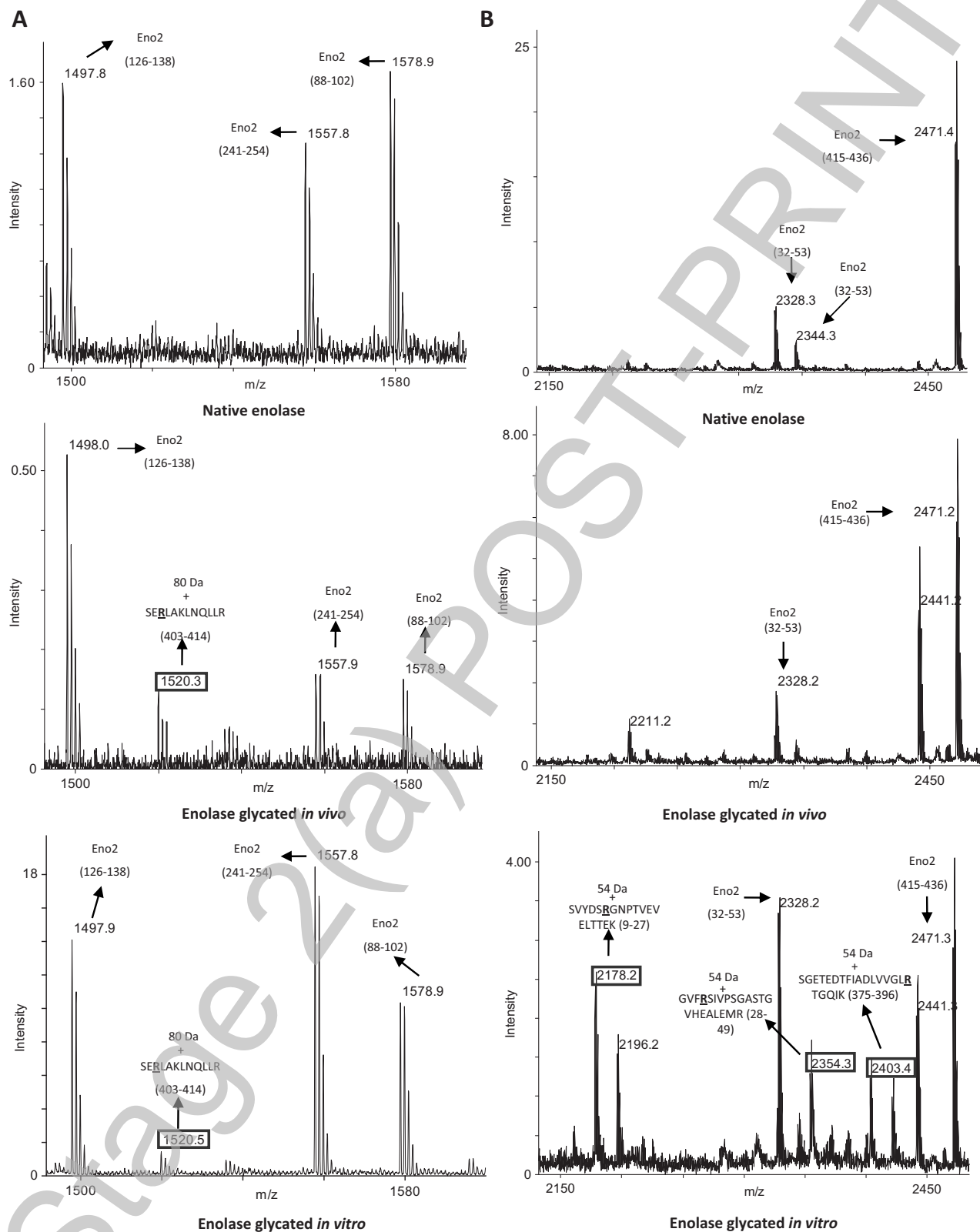
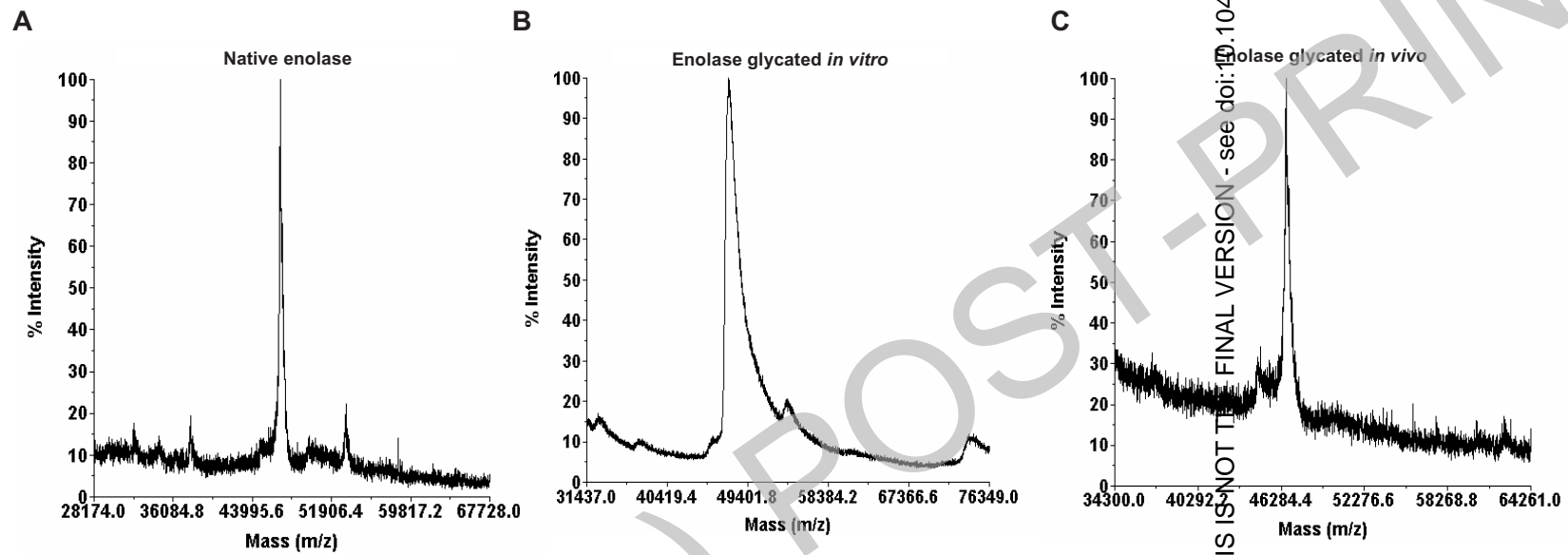


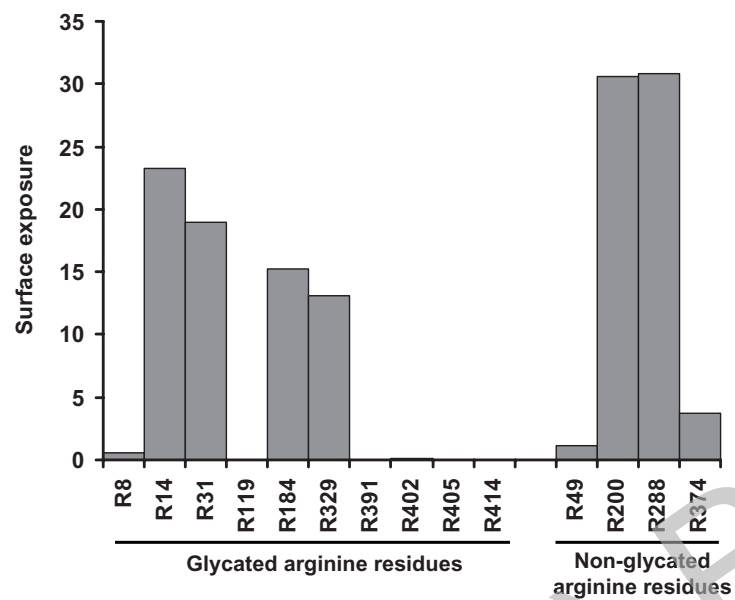
Figure 2



THIS IS NOT THE FINAL VERSION - see doi:10.1042/BJ20080632

Stage 2(a)

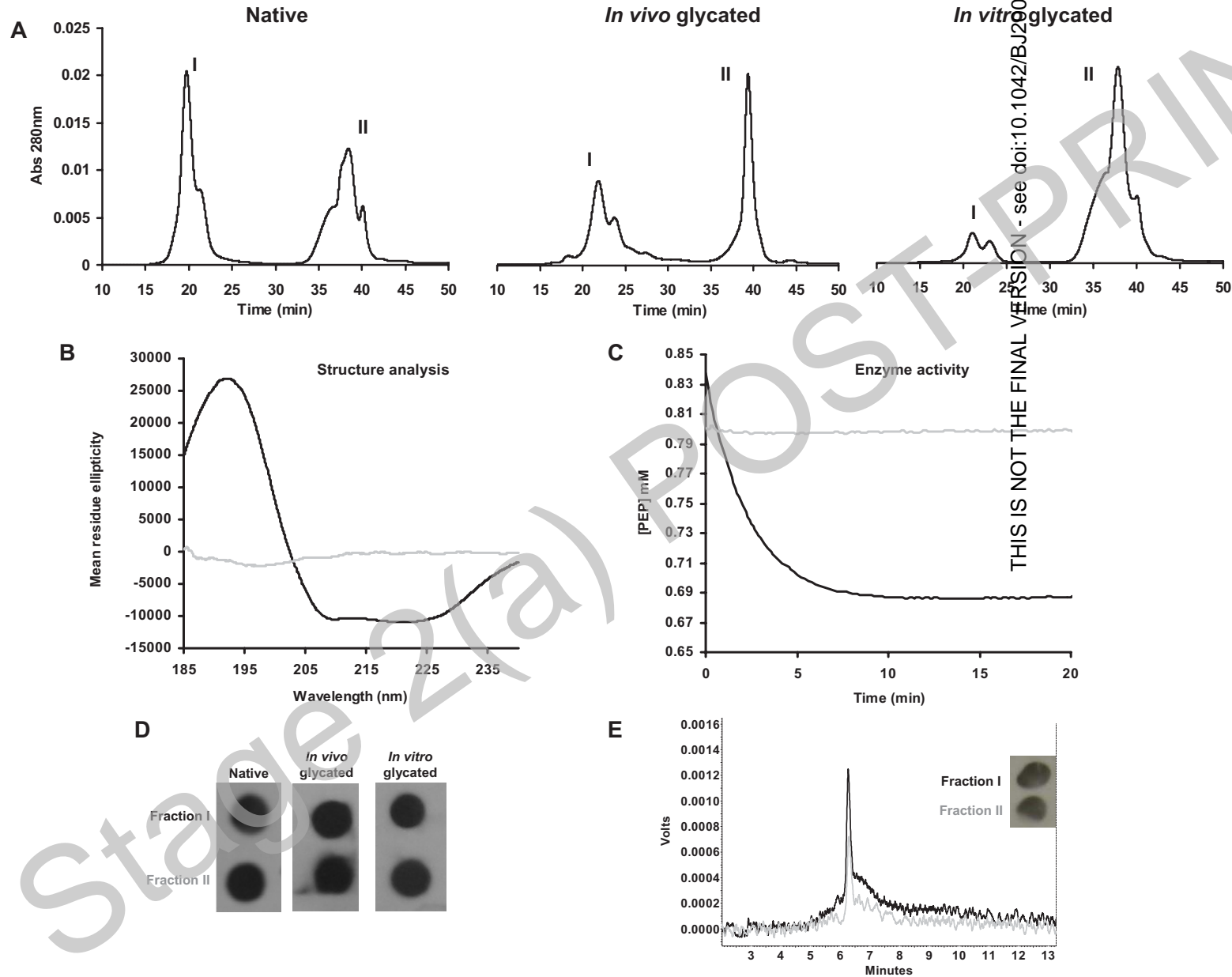
Figure 3



THIS IS NOT THE FINAL VERSION - see doi:10.1042/BJ20080632

Stage 2(a) POST-PRINT

Figure 4



THIS IS NOT THE FINAL VERSION - see doi:10.1042/BJ20080632

Figure 5

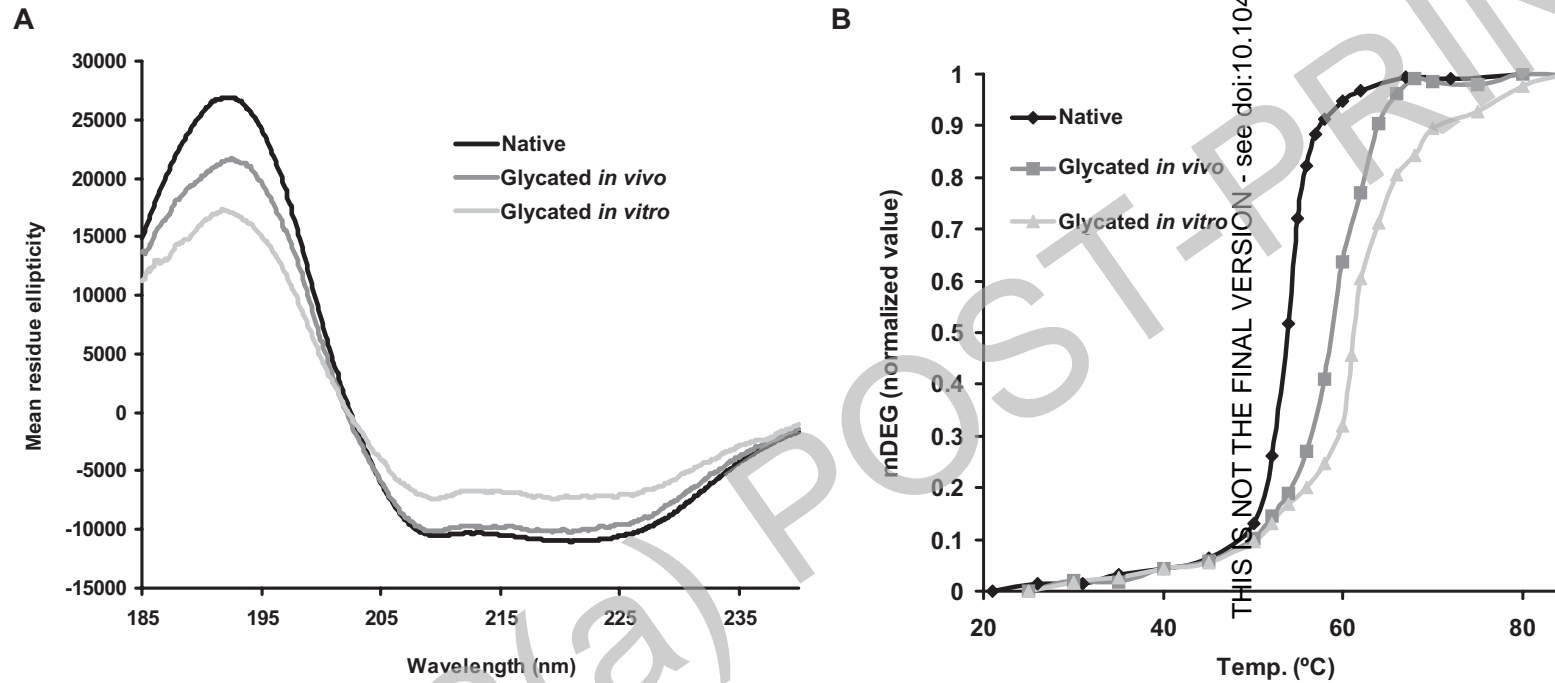
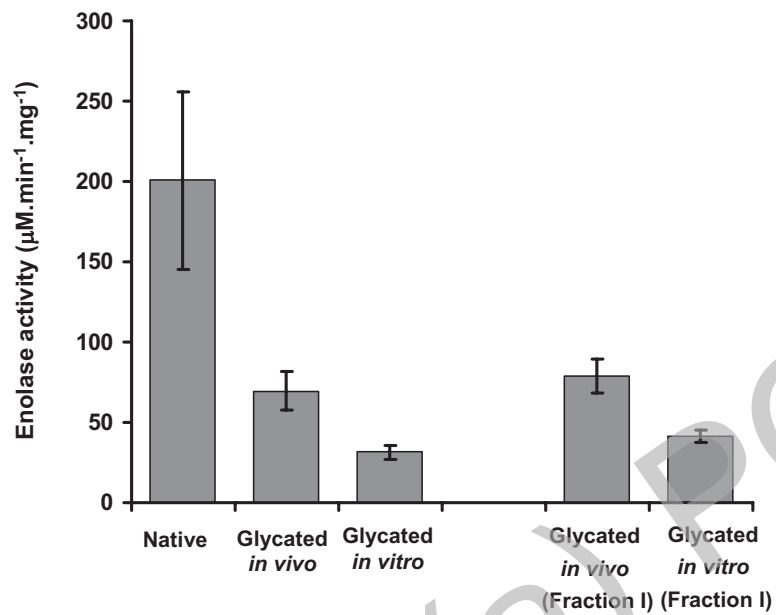


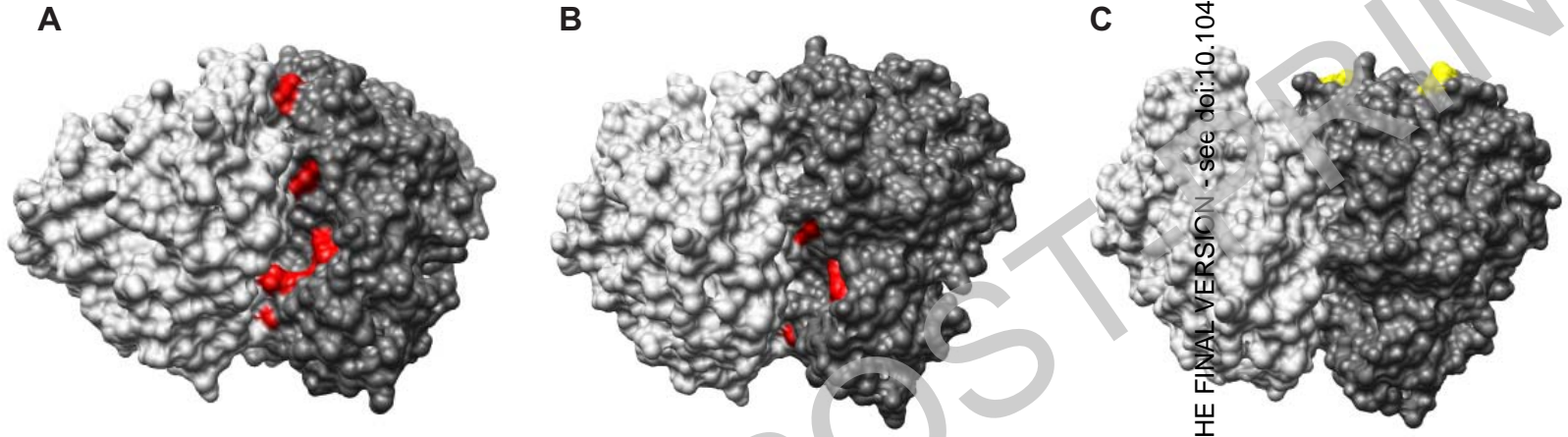
Figure 6



THIS IS NOT THE FINAL VERSION - see doi:10.1042/BJ20080632

Stage 2(a) PRE-POST-PRINT

Figure 7



THIS IS NOT THE FINAL VERSION - see doi:10.1042/BJ20080632

Stage 2(a) POST-PRINT

Table I

Glycation	Observed mass (Da)	Theoretical peptide mass (Da)	Peptide sequence	Mass increase (Da)	MAGE	Glycated residue
<i>In vitro</i>	1269.67	1215.61	VY <u>AR</u> SVYDSR (5-14)	54.01	MG-H	R8
	1310.63	1256.71	TGAP <u>AR</u> SE <u>RL</u> LAK (397-408)	54.01	MG-H	R402 or R405
	1520.14	1440.86	SE <u>RL</u> LAKLNQLLR (403-414)	80.03	Argp	R405
	1724.02	1669.92	LNQLL <u>RI</u> EEELGD K (409-422)	54.01	MG-H	R414
	1741.92	1669.03	IATAIE <u>KK</u> AADAL LLK (330-345)	72.02	CEL	K336 or K337
	2010.19	1956.07	LGANAILGVSM <u>AA</u> <u>AR</u> AAAAEK (105- 125)	54.01	MG-H	R119
	2020.12	1965.99	TFAEAM <u>RI</u> GSEVY HNLK (178-194)	54.01	MG-H	R184
	2178.18	2124.05	SVYDS <u>RG</u> NPTVEV ELTTEK (9-27)	54.01	MG-H	R14
	2354.32	2300.18	G <u>VF</u> RSIVPSGASTG VHEALEMR (28-49)	54.01	MG-H	R31
	2403.42	2349.23	SGETEDTFIADLV VGL <u>RT</u> GQIK (375- 396)	54.01	MG-H	R391
2635.57	2581.42	TAGIQIVADDLTV TNP <u>AR</u> IATAIEK (312-336)	54.01	MG-H	R329	
<i>In vivo</i>	1310.63	1256.71	TGAP <u>AR</u> SE <u>RL</u> LAK (397-408)	54.01	MG-H	R402 or R405
	1520.23	1440.86	SE <u>RL</u> LAKLNQLLR (403-414)	80.03	Argp	R405
	1741.90	1669.03	IATAIE <u>KK</u> AADAL LLK (330-345)	72.02	CEL	K336 or K337
	2252.20	2171.20	SKLGANAILGVSM AA <u>AR</u> AAAAEK (103-125)	54.01	MG-H	R119
	1750.00 [‡]	1669.96	LNQLL <u>RI</u> EEELGD K (409-422)	80.03	Argp	R414
	1654.83 [‡]	1600.84	AVSKVY <u>AR</u> SVYD SR (1-14)	54.01	MG-H	R8

[‡] Only observed by MALDI-FTICR-MS

Table II

Observed m/z	Charge	[M+H] ⁺	Theoretical peptide mass (Da)	Peptide sequence	Mass Increase (Da)	MAGE	Glycated residue
742.388	+3	2225.207	2171.196	SKLGANAILGVS MAAA R AAAAE K (103-125)	54.011	MG-H	R119
1005.508	+2	2010.080	1956.070	LGANAILGVSM AAA R AAAAEK (105-125)	54.011	MG-H	R119
772.375	+3	2315.239	2171.196	SKLGANAILGVS MAAA R AAAAE K (103-125)	144.042	THP	R119
1089.478	+2	2178.056	2124.046	SVYDS R GNPTV EVELTTEK (9-27)	54.011	MG-H	R14
726.67	+3	2178.056	2124.046	SVYDS R GNPTV EVELTTEK (9-27)	54.011	MG-H	R14
879.771	+3	2637.315	2583.305	SVYDSRGNPTVE VELTTEKGVFR (9-31)	54.011	MG-H	R14
756.68	+3	2268.088	2124.046	SVYDS R GNPTV EVELTTEK (9-27)	144.042	THP	R14
1010.459	+2	2019.996	1965.985	TFAEAM R IGSEV YHNLK (178-194)	54.011	MG-H	R184
1055.471	+2	2110.027	1965.985	TFAEAM R IGSEV YHNLK (178-194)	144.042	THP	R184

Table III

Structural elements	α -Helix	β -Sheet	β -Turns	Unordered structure	NRMSD
Native	0.40	0.20	0.21	0.19	0.011
Glycated <i>in vivo</i>	0.35	0.20	0.20	0.25	0.017
Glycated <i>in vitro</i>	0.17	0.32	0.19	0.32	0.026